

Received January 24, 2022, accepted February 11, 2022, date of publication February 22, 2022, date of current version March 2, 2022.

Digital Object Identifier 10.1109/ACCESS.2022.3153710

# Compact Microstrip Wideband Cross-Coupled Inline Bandpass Filters With Miniaturized Stepped-Impedance Resonators (SIRs)

SHAO-CHAN TANG<sup>1</sup>, PEI-CHENG CHU<sup>2</sup>, JEN-TSAI KUO<sup>1,2</sup> , (Fellow, IEEE), LIN-KUN WU<sup>1</sup>, (Member, IEEE), AND CHUN-HUNG LIN<sup>2</sup>

<sup>1</sup>Institute of Communications Engineering, College of Electrical and Computer Engineering, National Yang Ming Chiao Tung University, Hsinchu 30010, Taiwan

<sup>2</sup>Department of Electronic Engineering, Chang Gung University, Taoyuan 33302, Taiwan

Corresponding author: Jen-Tsai Kuo (jtkuo123@mail.cgu.edu.tw)

This work was supported in part by the Ministry of Science and Technology, Taiwan, under Grant MoST 110-2221-E-182-021; and in part by Chang Gung University under Grant BMRPB95.

**ABSTRACT** This paper presents a class of reduced footprint inline microstrip bandpass filters capable of covering bandwidth up to 20% as well as good flexibility in establishing various cross-couplings for creating transmission zeros. The resonating elements are quarter-wave stepped-impedance resonators (SIRs), which have a wide upper stopband in nature. To achieve size miniaturization, the low-impedance segment of each SIR is implemented as a thick-trace ring and configured in a spiral form, and the high-impedance section is deformed to accommodate the low-impedance section. An interlaced coupling structure is proposed to enhance the coupling limited by the downsized coupled segments of adjacent resonators. In addition, by properly routing the associated shorted stubs, the structure can easily establish cross-coupling between nonadjacent resonators. Thus, compact SIR filters in an inline arrangement can be achieved to have either narrow or wide passbands with multiple transmission zeros. Two such circuits with sharp transition bands and upper stopband extension are synthesized, fabricated, and tested. The measured results show good agreement with simulated data. The circuit areas together with the performances of the experimental filters are compared with those in existing literature.


**INDEX TERMS** Bandpass filter, compact, cross-coupling, microstrip, miniaturization, stepped-impedance resonator (SIR), transmission zero, wideband.

## I. INTRODUCTION

Bandpass filter (BPF) is an essential device in the RF front end of a wireless/microwave communication system for rejecting unwanted out-of-band signals. One of the key metrics for characterizing a practical BPF is circuit miniaturization, and the design challenge lies in satisfying the trade-off among insertion loss, achievable bandwidth, and upper stopband extension [1]. The circuit size reduction often relies on the miniaturization techniques of individual resonator, such as hairpin resonators [2], stepped-impedance resonators (SIRs) [3], and hybrid-resonance resonators [4]. In general, downsized resonators will pose a constraint on achievable circuit bandwidth since the coupling strength is limited. Good examples are the filters in [2]–[4], of which the

fractional bandwidths (FBWs) are less than 10%. In addition, frequency selectivity in transition band is also one of important concerns in filter design. To enhance the selectivity, more resonating elements can be used, but this will lead to increased both circuit area and insertion loss. For enhancing out-of-band rejection and saving the in-band insertion loss, cross-couplings are widely used in filter synthesis [5], [6] for creating transmission zeros. In practice, cross-coupled resonators are usually arranged in a symmetric double array; hence, the whole structure can be bulky. Furthermore, cross-couplings usually require fine layout geometries in realization, and hence time-consuming EM simulations.

Recently, filters with inline configuration regain much attention due to its compact size and good electrical and physical isolation between input and output (I/O) ports [7], [8]. To minimize the circuit order and to realize satisfactory frequency selectivity in transition bands, the

The associate editor coordinating the review of this manuscript and approving it for publication was Dušan Grujić .

following three design approaches are adopted for generating transmission zeros. The first one is based on the extracted-pole synthesis with nonresonating nodes (NRNs) [9], [10]. The second method uses frequency-dependent couplings [11], [12]. In practice, this type of coupling is realized by mixed electric and magnetic couplings between resonators [7], [13]–[16]. The third approach is to add extra cross-coupling paths [8], [17]. It is noted that most inline designs in literature are basically for cavity filters; only a small number of papers have extended such techniques to planar applications. It is worth mentioning that the achievable bandwidth and flexibility in allocating transmission zeros of the inline designs in [7]–[17] are limited. For example, only [14] has an experimental filter with an FBW larger than 10%.

The demand of extended upper stopband is also increasing for eliminating interferences from adjacent channels or other wireless systems. It is known that SIR is a good candidate for realizing a wide stopband response [3], [18]–[19]. In [18], a compact trisection filter based on net-type resonators is realized to have a spurious resonance at  $6.5f_0$  with an area of only  $0.15\lambda_g \times 0.15\lambda_g$  ( $\lambda_g$  is the guided wavelength at the design frequency). This structure, however, seems limited to narrowband applications since each coupling arm is less than  $0.1\lambda_g$ . In [19], the proposed interdigital SIR filters not only preserve the advantage of a very compact size and wide upper stopband but also resolve the problem of limited coupling strength with adjacent conventional quarter-wave SIRs. However, both accuracy and time of EM simulations of the sophisticated structure will be tough issues. The primitive of short-circuited stub-embedded ring resonators in [20] is an SIR. Its circuit area is small and FBWs of the realized diplexer are less than 5%, due to the limited coupling geometries, as expected. Besides SIRs, the structures in [21]–[25] have been proposed to implement a wideband BPF with a wide stopband response.

The primary purpose of this paper is to show the development of highly compact planar inline filters suitable for realizing transmission zeros with cross-couplings as well as bandwidths up to 20%. The resonating elements are quarter-wave SIRs. The low-impedance section is deformed into a spiral ring so that the whole circuit area can be significantly reduced, and the thin grounded high-impedance tail is flexibly routed for implementing cross-couplings in the inline structure.

The paper is organized as follows. Section II describes resonance characteristics of the proposed SIR, together with geometry control for area shrinking and inter-resonator couplings. Section III depicts the synthesis and design of the inline wideband filters with cross-couplings. For demonstration, two filters are fabricated and measured. One is a trisection with a transmission zero in the upper stopband, and the other is a sixth-order filter with two pairs of transmission zeros. Both experimental circuits are designed to have a bandwidth greater than 20%, even though their circuit sizes are highly miniaturized. Measurement results are

compared with simulation responses, and then some practical issues in filter realization are also discussed. Section IV draws the conclusion.

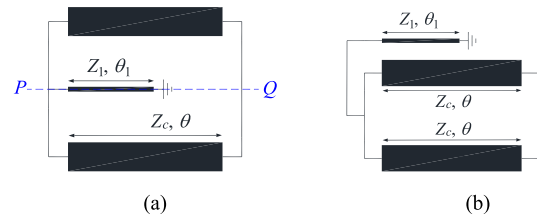


**FIGURE 1.** The proposed resonator. (a) Shorted stub inside the ring for circuit miniaturization. (b) Shorted stub outside the ring for establishing appropriate couplings.

## II. RESONATOR, MINIATURIZATION, AND COUPLING

Fig. 1 shows the circuit schematics of the proposed quarter-wave SIR. It is formed by a low-impedance closed ring tapped with a high-impedance shorted stub at  $P$ , where  $PQ$  is its symmetry plane. The characteristic impedances and electrical lengths are also given in Fig. 1. The shorted stub can be either placed inside the ring, as in Fig. 1(a), for circuit miniaturization or outside the ring, as in Fig. 1(b), for establishing appropriate couplings with other resonators. The resonator in Fig. 1(a) is the same as the short-circuited stub-embedded ring resonator of type A in [20]. In comparison with [20], as it will be shown later, our realization of Fig. 1 is not only much smaller but also capable of building filters with relatively wide bandwidths and flexible cross-couplings for generating transmission zeros.

### A. RESONANCE CHARACTERISTICS

The resonance frequencies of the resonator proposed in Fig. 1 can be easily determined by subsequently replacing the  $PQ$ -plane with a magnetic and electric wall. It results in the following resonance conditions

$$R = \tan\theta_1 \tan\theta \quad (\text{Even mode}) \quad (1a)$$

$$\theta = n\pi, \quad n = 1, 2, 3, \dots \quad (\text{Odd mode}) \quad (1b)$$

where  $R = Z_c/(2Z_1)$ . It is easily seen that the even-mode resonance condition (1a) is the same as that of a quarter-wave SIR [3], where  $2Z_1$  is the characteristic impedance of the bisected high-impedance section. Condition (1b) is obtained by shorting the  $Z_1$ -section to ground, which represents the natural resonances of the low-impedance segment. A simple root-searching program can be used to calculate the resonance frequencies based on the two conditions. Fig. 2 plots the leading two higher-order resonances  $f_1$  and  $f_2$  normalized with respect to their associated fundamental resonance  $f_0$  as a function of length ratio  $u = \theta_1/(\theta_1 + \theta)$ , where  $f_0$  and  $f_2$  are from (1a), and  $f_1$  from (1b).

In Fig. 2, it is found that  $f_1 > f_2$  when  $u > u_x = 1/3$ . It can be validated that the boundary  $u_x$  is independent of the value of  $R$ . By choosing  $u = 1/2 > u_x$ , i.e.,  $\theta_1 = \theta$ , for any  $R < 1$ , not only  $f_2$  reaches its highest point, but also  $f_1 > f_2$ . Since any higher-order resonances may cause spurious

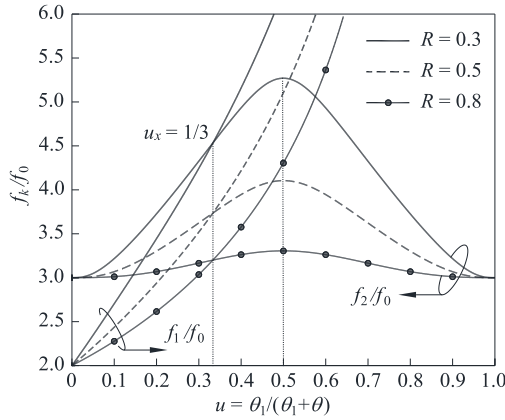


FIGURE 2. Normalized frequencies of the leading two higher-order resonances for the resonator proposed in Fig. 1.  $R = 0.3, 0.5,$  and  $0.8$ .

$S_{21}$  peaks in the upper stopband, this suggests the fact that  $u = 1/2$  should be selected for the best filter performance in the upper rejection band. This choice is the same as that in [3], even when the low-impedance segment of the proposed SIR is deformed. It also can be seen from Fig. 2 that the smaller the  $R$  value, the shorter the total SIR length. Take  $R = 0.3$  as an example. By inserting the shorted stub in the ring in Fig. 1(a), the total electrical length of the resonator at the fundamental resonance is only  $\theta = \theta_1 = 28.71^\circ$ , which is merely one twelfth of a wavelength. The ring also contributes further reduction, as it reduces value of  $R$  from  $Z_c/Z_1$  to  $Z_c/(2Z_1)$ . In addition to size reduction, the use of the ring brings additional advantages. Usually, width of the high impedance section approaches the fabrication limit, which may decrease the unloaded  $Q$  of the SIR. Alternatively, keeping the high-impedance section “moderately” thin, one can adopt a sufficiently low  $Z_c$  value to meet the impedance ratio  $R$  in need. Yet when the line width of the low-impedance section gets close to the length, spurious transversal resonances might occur and degrade the performance. The low-impedance section in a ring form will be free of such degradations, gaining desired impedance ratio while keeping both  $Z_c$  and  $Z_1$  reliable and feasible. In addition, the ring section possesses a better routing efficiency than conventional SIRs since the ring trace can be easily folded into an arbitrary shape. This is also helpful for establishing desired direct as well as cross-couplings of either electric or magnetic type [5].

**B. CIRCUIT MINIATURIZATION**

To make a significant circuit area reduction, the double-ring spiral configuration [26] is employed for the low-impedance ring in Fig. 1, as shown in Fig. 3. The ring peripheral is folded into two spiral loops with a short CPW section etched on the ground plane as the interconnection. The line width  $W_c$  and the gap size  $s$  of the CPW is designed to match the characteristic impedance of the microstrip traces on the top layer for minimizing the discontinuity. The black traces denote top metal, the gray area indicates the bottom ground conductor, and the white circular dots represent either

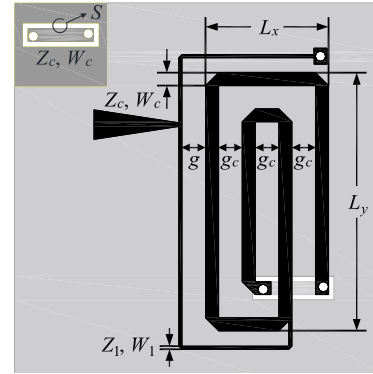


FIGURE 3. Schematic of a double-ring spiral resonator.

signal vias connecting traces on the top and bottom layers or grounding via for the shorted stub.

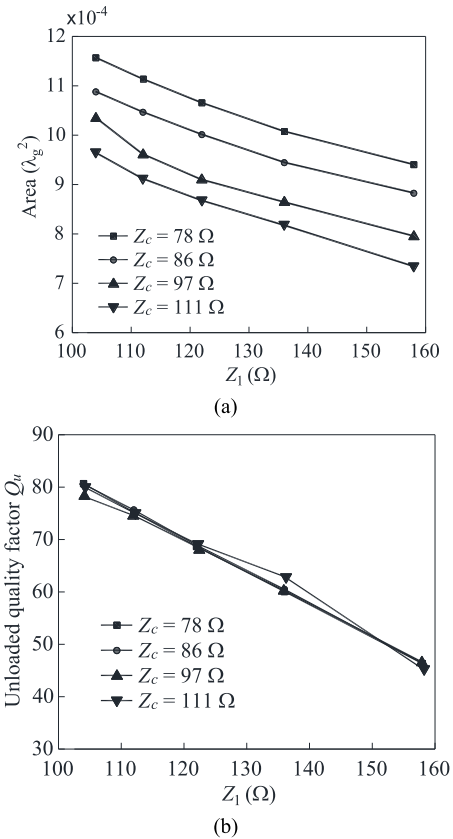
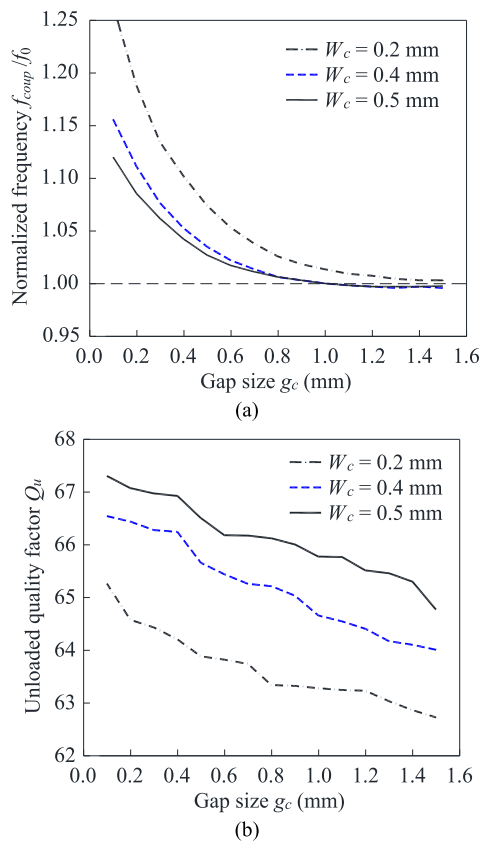


FIGURE 4. Design curves of the resonator proposed in Fig. 3. (a) Area. (b) Unloaded quality factor  $Q_u$ .

By aligning the shorted stub along the ring peripheral, in Fig. 3, the area occupied by a single resonator is approximately equal to that of the spiral ring. Define a length-to-width ratio  $r = L_y/L_x$ , it can be known from Cauchy-Schwarz inequality that when  $r = 1$  the area has its maximum, and the area can be significantly scaled down when  $r \gg 1$ . Herein, all gaps between ring traces are initially set as  $g_c = 0.2$  mm (conservative resolution for reliable fabrication) to minimize the circuit area. Fig. 4(a) plots the area, in terms of  $\lambda_g^2$ , of a single resonator on a Rogers RO4003C substrate

with  $\epsilon_r = 3.38$ ,  $h = 20$  mil, and metal thickness  $t = 18 \mu\text{m}$  against different  $Z_1$  and  $Z_c$  values. Theoretically, lower  $R$  will result in a more compact size. When  $Z_c$  is kept constant, the downward trend of circuit size can be observed as  $Z_1$  is increased from  $104 \Omega$  to  $158 \Omega$ . Yet, as  $Z_c$  is decreased from  $111 \Omega$  to  $78 \Omega$ , for a constant  $Z_1$ , the area increases. This is attributed to the increase of line width of the ring trace in practice. The simulation data are obtained by a full-wave package IE3D [27]. Fig. 4(b) illustrates the unloaded quality factor  $Q_u$  versus different geometries. As  $Z_1$  increases,  $Q_u$  decreases from 80 to 46; however, the variation of  $Z_c$  does not make significant difference in  $Q_u$ . Fig. 4 also reveals that the smaller the resonator, the lower the  $Q_u$ .



**FIGURE 5.** Resonance characteristics of the resonator proposed in Fig. 3 versus  $g_c$ . (a) Normalized resonance frequency  $f_{coup}/f_0$ . (b) Unloaded quality factor  $Q_u$ .

To attain a highly compact SIR, the separation between lines  $g_c$  in Fig. 3 is made as small as possible. Fig. 5 investigates the influence of possible couplings among the segments within the spiral ring on the resonance frequency, where the effect of right-angle bends is also taken into consideration in simulation. Fig. 5(a) shows the variation of normalized resonance frequencies  $f_{coup}/f_0$  with respect to the change of  $g_c$ . Given  $W_c = 0.2, 0.4$ , and  $0.5$  mm and  $W_1 = 0.1$  mm, the frequency shift from  $f_0$  is less than 5% when  $g_c > 0.6, 0.4$ , and  $0.3$  mm, respectively. When  $g_c = 0.1$  mm,  $f_{coup}$  can be 12% – 25% higher than  $f_0$ . This means that when  $g_c$ , and hence  $L_x$ , is decreased,  $L_y$  will be increased to tune the resonance back to  $f_0$ . Surprisingly, such increase in  $L_y$  does not exceed

the decrease in  $L_x$  since there are three  $g_c$ 's within the spiral ring, where a small change in  $g_c$  actually makes a significant change in  $L_x$ . As a result, for  $W_c = 0.5$  mm, the area of a resonator is reduced from  $48.63 \lambda_g^2$  to  $34.27 \lambda_g^2$ , which is an additional 30% reduction when  $g_c$  is changed from 1.5 mm to 0.1 mm.

Fig. 5(b) displays the unloaded quality factor  $Q_u$  of the SIR versus  $g_c$ . It indicates that  $Q_u$  falls in a range from 62 to 68. As  $g_c$  is increased from 0.1 mm to 1.5 mm, the three  $Q_u$  sets all decrease by about 4%. At any given  $g_c$ , resonators with the thinnest ring trace exhibit the lowest  $Q_u$ , as expected.

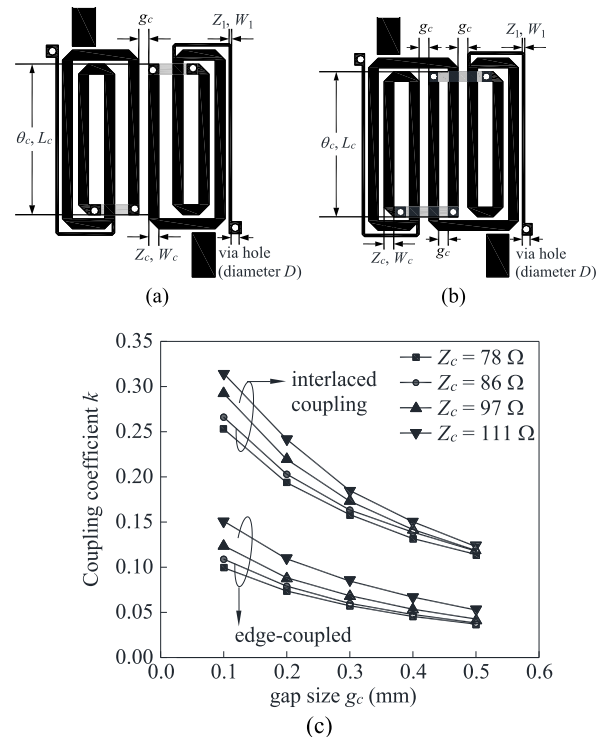


**FIGURE 6.** Coupling structures and design curves. (a) Edge-coupled. (b) Interlaced coupling. (c) Coupling coefficients design curves. Substrate RO4003C is used.  $L_c = 8$  mm and  $W_1 = 0.13$  mm.

### C. COUPLING STRUCTURE

Fig. 6 shows the two coupling structures employed in our designs. In Fig. 6(a), the coupling is realized by the outermost ring traces of two neighboring resonators. The coupling length is merely  $0.043\lambda_g$  at the design frequency  $f_0 = 1$  GHz, so that the coupling strength is limited. In Fig. 6(b), the positions of the two coupling arms in Fig. 6(a) are interchanged, forming an interlaced coupling structure like the Lange coupler [28], to enhance the coupling.

The coupling coefficients  $k$  of the two coupling structures in Fig. 6(a) and 6(b) are extracted by the weak coupling method [5]. Fig. 6(c) illustrates the variation of coupling coefficient  $k$  versus  $g_c$  for  $Z_1 = 132 \Omega$ , where  $Z_c = 78, 86, 97$ , and  $111 \Omega$ . The coupling coefficients of both structures decrease as the gap size  $g_c$  is increased. For the same  $Z_c$  and  $g_c$  in Fig. 6(c),  $k$  values of the interlaced coupling structure are more than two times those of the edge-coupled structure in

Fig. 6(a). Thus, the coupling coefficient covers a range from lower than 0.05 to higher than 0.3. This reflects the fact that the proposed coupling structure is also suitable for design of circuits with relatively wide bandwidths. It is noted that the areas used by these two coupling structures are approximately the same.

### III. TWO EXPERIMENTAL INLINE FILTERS

A trisection and a sixth-order inline filter are realized for demonstration. Also described is the implementation of extra cross-coupling with appropriate polarities in these two inline filters for creating transmission zeros at designated positions. The circuits are designed on a Rogers RO4003C substrate with  $\epsilon_r = 3.38$ ,  $h = 20$  mil, metal thickness  $t = 18 \mu\text{m}$ , and loss tangent  $\tan\delta = 0.0021$ . The initial electrical parameters for all resonators are  $Z_1 = 132 \Omega$ ,  $Z_c = 78 \Omega$ , and  $u = 0.5$  before the whole filter is simulated for final fine tuning. The width of the shorted stub  $W_1 = 0.12$  mm is close to the fabrication limit of standard PCB process.

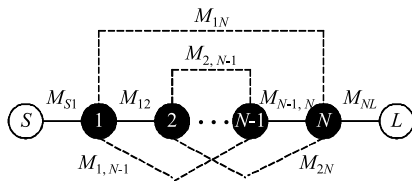


FIGURE 7. Coupling scheme for an  $N^{\text{th}}$ -order cross-coupled inline filter.

Fig. 7 shows a generic  $N^{\text{th}}$ -order coupling scheme of an inline filter. Each dark dot represents a resonator, empty circles stand for the I/O ports, the solid lines  $M_{ij}$  denote inter-resonator mainline couplings, and the dashed lines mean cross-couplings. The corresponding  $(N + 2) \times (N + 2)$  coupling matrix can be established by the synthesis procedure in [6], and the response can be obtained by the conventional lowpass-to-bandpass transformation [28, eq. (8.71)]. In the bandpass domain, the corresponding coupling coefficient between resonators  $i$  and  $j$ ,  $k_{ij}$ , and external quality factor  $Q_{ext}$  of the first and last resonators can be written as [5, eq. (7.9) and (7.84)]

$$k_{ij} = M_{ij} \times \Delta \tag{2a}$$

$$Q_{ext} = 1/(M_{S1}^2 \times \Delta) \tag{2b}$$

where  $\Delta$  is the FBW.

#### A. WIDEBAND TRISECTION

The first experimental circuit is a trisection filter for demonstrating a wideband application. The passband at center frequency  $f_0 = 1$  GHz has a 0.1-dB ripple and fractional bandwidth  $\Delta = 21\%$ . The coupling coefficients in the bandpass domain can be obtained as  $k_{12} = k_{23} = -0.2133$  and  $k_{13} = 0.0177$  [5]. The interlaced coupling structure in Fig. 6(b) is used to realize  $k_{12}$  and  $k_{23}$  with  $L_c = 8$  mm and  $g_c = 0.2$  mm. Fig. 8(a) shows the circuit layout. The cross-coupling  $k_{13}$  should be positive for creating a transmission zero. It is implemented by bringing the shorted high-impedance sections of the two end resonators

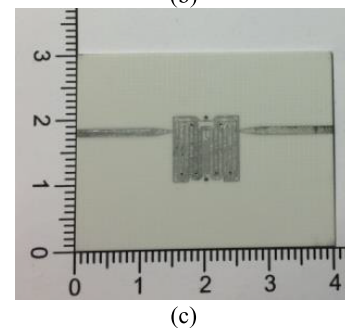
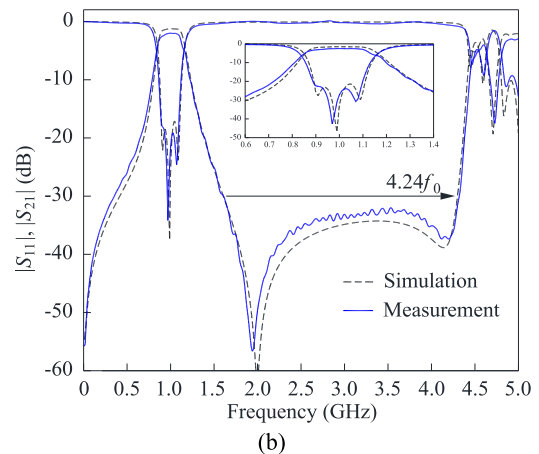
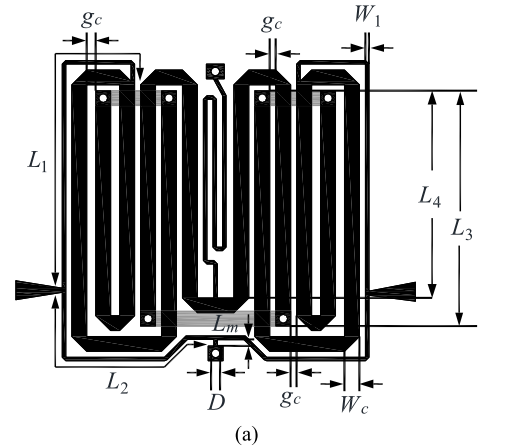


FIGURE 8. Miniaturized wideband inline trisection filter. (a) Circuit layout. (b) Simulated and measured responses. (c) Photograph of the measured circuit. Geometric parameters in mm:  $L_1 = 7.40$ ,  $L_2 = 10.50$ ,  $L_3 = 7.94$ ,  $L_4 = 6.99$ ,  $L_m = 0.22$ ,  $W_1 = 0.12$ ,  $W_c = 0.50$ ,  $g_c = 0.20$ , and  $D = 0.30$ .

together and leaving a common short high-impedance section  $L_m = 0.22$  mm before they are connected to the grounding via. A tapped-line feeding is applied to match the external quality factor of these two resonators.

Fig. 8(b) compares measured responses with the simulated data of the fabricated circuit. The measured in-band insertion loss is 2.05 dB, the fractional bandwidth  $\Delta = 21.5\%$ , and the return loss is better than 18 dB. The transmission zero is at  $1.96$  GHz due to the inductive cross-coupling. The upper stopband is extended to  $4.24f_0$  for a reference rejection level of 30 dB. The circuit area is only  $0.053\lambda_g \times 0.053\lambda_g (10.26 \times 10.13 \text{ mm}^2)$ . Good agreement



between the simulation and measured responses is obtained. Fig. 8(c) shows the photograph of the measured circuit.

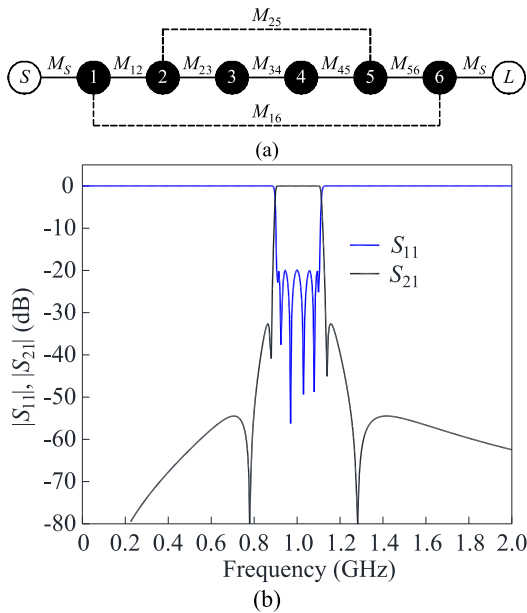


FIGURE 9. Inline sixth-order canonical filter. (a) Coupling scheme. (b) Calculated  $S$ -parameter responses by the coupling matrix in (3).

**B. INLINE SIXTH-ORDER CANONICAL FILTER**

The second design is an inline sixth-order circuit with four transmission zeros. The circuit topology, as shown in Fig. 9(a), can generate two pairs of transmission zeros. The corresponding coupling matrix is given below

$$[M] = \begin{bmatrix} 0 & M_S & 0 & 0 & 0 & 0 & 0 & 0 \\ M_S & 0 & M_{12} & 0 & 0 & 0 & M_{16} & 0 \\ 0 & M_{12} & 0 & M_{23} & 0 & M_{25} & 0 & 0 \\ 0 & 0 & M_{23} & 0 & M_{34} & 0 & 0 & 0 \\ 0 & 0 & 0 & M_{34} & 0 & M_{45} & 0 & 0 \\ 0 & 0 & M_{25} & 0 & M_{45} & 0 & M_{56} & 0 \\ 0 & M_{16} & 0 & 0 & 0 & M_{56} & 0 & M_S \\ 0 & 0 & 0 & 0 & 0 & 0 & M_S & 0 \end{bmatrix} \quad (3)$$

In the lowpass domain, the designated zeros are at  $\Omega = \pm 1.3$  and  $\pm 2.5$ , and the coupling coefficients  $M_S = 0.9925$ ,  $M_{12} = M_{56} = -0.8248$ ,  $M_{23} = M_{45} = -0.5509$ ,  $M_{34} = -0.7591$ ,  $M_{25} = 0.2387$ , and  $M_{16} = -0.0242$ . Given the FBW  $\Delta = 20\%$ , the coupling coefficients of the filter are  $k_{12} = k_{56} = -0.1650$ ,  $k_{23} = k_{45} = -0.1102$ ,  $k_{34} = -0.1518$ ,  $k_{25} = 0.0477$ ,  $k_{16} = -0.0048$ ,  $Q_{ext} = 5.08$ , and the zeros are at 0.78, 0.88, 1.14, and 1.28 GHz. Fig. 9(b) shows the calculated  $S$ -parameters.

As indicated by the circuit layout in Fig. 10(a), all the resonators are arranged in an inline configuration, instead of a two-dimensional array. The mainline couplings are of the same polarity and have relatively large magnitudes, and they are realized by capacitive couplings by the interlaced

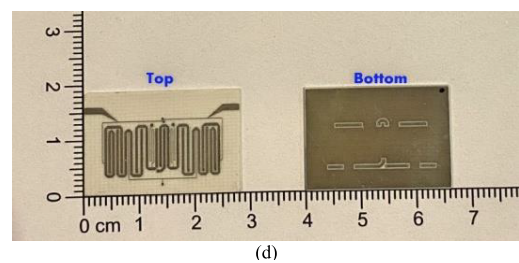
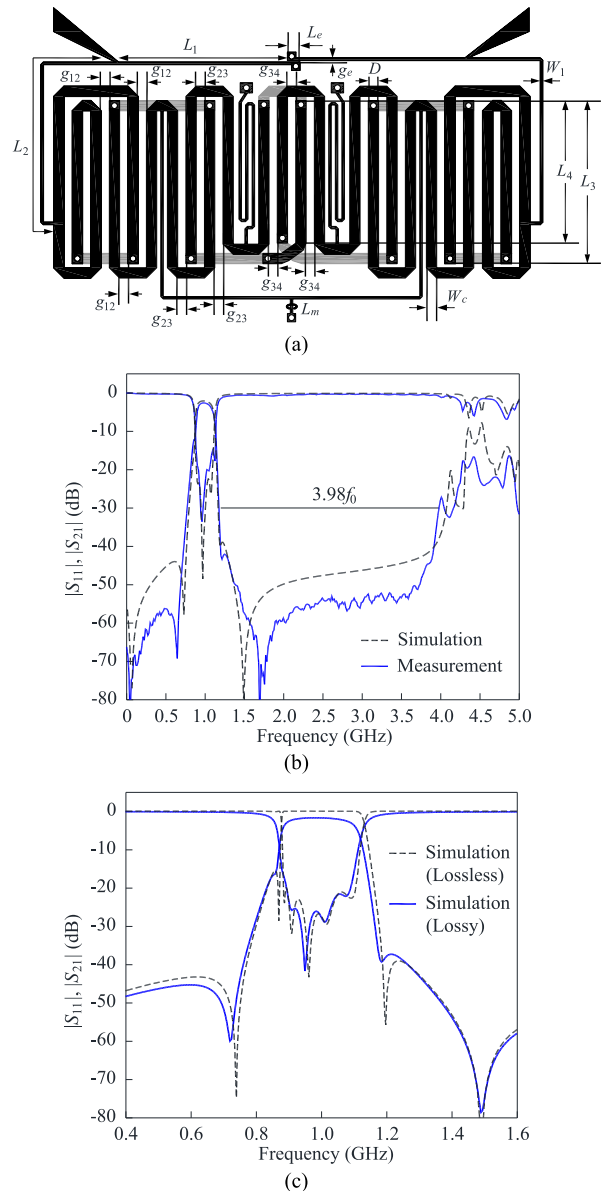


FIGURE 10. Sixth-order inline canonical filter. (a) Circuit layout. (b) Wideband simulated and measured results. (c) Simulated in-band responses with/without substrate loss. (d) Photograph of the measured circuit. Geometric parameters in mm:  $L_1 = 7.66$ ,  $L_2 = 10.21$ ,  $L_3 = 7.94$ ,  $L_4 = 6.94$ ,  $L_m = 0.71$ ,  $L_e = 0.60$ ,  $W_1 = 0.12$ ,  $W_c = 0.5$ ,  $W_m = 0.12$ ,  $g_{12} = 0.23$ ,  $g_{23} = 0.42$ ,  $g_{34} = 0.20$ ,  $g_e = 0.13$ , and  $D = 0.30$ .

coupling structure in Fig. 6(b). The required inductive cross-coupling  $M_{25}$  is implemented by a shorted high impedance section, whereas the anti-phase coupling  $M_{16}$  is realized

TABLE 1. Performance comparison with existing BPFs in literature.

Reference	Order	No. of Zeros	IL (dB)	$\Delta$ (%)	Spurious frequency	Circuit dimension ( $\lambda_g^2$ )	Circuit area ( $\lambda_g^2 \times 10^{-4}$ )
[4]	2	1	2.30	4.2	$2.61f_0$ (15 dB)	$0.1440 \times 0.1280$	184.3
[4]	4	1	2.03	10	$2.86f_0$ (20 dB)	$0.2170 \times 0.1000$	217.0
[18]	3	1	2.80	4.7	$6.5f_0$ (30 dB)	$0.1500 \times 0.1500$	225.0
[19]	4	2	0.64	59.2	$5.12f_0$ (20 dB)	$0.0654 \times 0.0833$	54.5
[20]	3	1/1	1.2/1.3	4.1/3.6	$3.0f_0$ (30 dB)	$0.4200 \times 0.1570$	659.4
[22]		2	0.80	101.9	$3.71f_0$ (20 dB)	$0.2400 \times 0.1900$	456.0
[23]			0.30	123	$4.50f_0$ (30 dB)	$0.1700 \times 0.1400$	238.0
[24]		4	0.85	44	$2.15f_0$ (30 dB)	$0.1500 \times 0.1000$	150.0
[25]		4	0.53	77.5	$5.38f_0$ (30 dB)	$0.0900 \times 0.1580$	142.2
This work	3	1	2.05	21	$4.24f_0$ (30 dB)	$0.0530 \times 0.0530$	28.1
This work	6	4	2.61	20	$3.98f_0$ (30 dB)	$0.1182 \times 0.0663$	78.4

by a pair of short-ended parallel-coupled lines [29]. The simulated and measured results from 0 to 5 GHz are plotted in Fig. 10(b), showing a stopband extension to  $3.98f_0$  for a reference level of 30 dB. The minimum measured in-band insertion loss is 2.61 dB, and the measured fractional bandwidth is 24%. The return loss in the passband is better than 15 dB. Four transmission zeros are at 0.65, 0.86, 1.22, and 1.70 GHz. Good agreement between measured and simulated results can be observed. The frequency shift may be attributed to unwanted stray coupling between nonadjacent resonators since the twisted loops have a tight layout arrangement. Also, coupling between thin traces and dielectric losses will degrade the quality factors of the resonators, leading to deterioration of the stopband attenuation compared to calculated results in Fig. 9(b). Fig. 10(c) illustrates the comparison between simulation data with and without substrate loss. It indicates that substrate loss not only degrades the passband but also the stopband attenuation at each transmission null. The circuit area is only  $0.1182\lambda_g \times 0.0663\lambda_g$ . Fig. 10(d) shows the photograph of the measured circuit.

Table 1 compares the performances of the proposed compact inline BPFs with those in some previous works. The fourth-order circuit in [4] has merely a transmission zero, and its FBW is limited by 10%. More importantly, its circuit area is more than 2.5 times that of the six-order filter in Fig. 10(d). Significant improvement in stopband performance can be observed from [4] to both the trisection and sixth-order filters, even though a more stringent level of 30 dB is referred here. The trisection in [18] has the best stopband performance among all works cited in Table 1. Due to its multi-stubs, however, not only the achievable circuit bandwidth is restricted, but also the circuit area is eight times of that of the trisection in Fig. 8(c). The circuit in [19] features the best insertion loss, but it lacks design flexibility for a higher roll-off rate or more zeros. For the UWB applications in [22]–[25], the FBW is wider than those of our work; however, their areas are comparatively larger. As it can be seen from Table 1, the proposed BPFs have a noteworthy significance in both number of transmission zeros and circuit area reduction. The presented design is also suitable for a relatively wide passband up to more than 20%.

#### IV. CONCLUSION

Very compact inline planar bandpass filters are realized with cross-couplings and wide bandwidth utilizing highly miniaturized SIRs. Some design curves are provided to show how to determine the impedance ratio compromised for both size reduction and upper stopband extension. A novel interlaced coupling structure is exploited to extend the coupling level of the miniaturized resonators, enabling applications requiring a wider operation bandwidth. An additional significantly important feature of the proposed resonators is that the shorted high-impedance stubs can provide inductive as well as capacitive cross-couplings, and consequently save much area for extra cross-couplings for creating transmission zeros. A trisection and a sixth-order inline filter are synthesized and realized for validating the idea, showing the flexibility of the proposed resonators in filter design. The measured results show a good agreement with the simulation.

#### REFERENCES

- [1] R. V. Snyder, G. Macchiarella, S. Bastioli, and C. Tomassoni, "Emerging trends in techniques and technology as applied to filter design," *IEEE J. Microw.*, vol. 1, no. 1, pp. 317–344, Jan. 2021.
- [2] M. Sagawa, K. Takahashi, and M. Makimoto, "Miniaturized hairpin resonator filters and their application to receiver front-end MICs," *IEEE Trans. Microw. Theory Techn.*, vol. 37, no. 12, pp. 1991–1997, Dec. 1989.
- [3] J.-T. Kuo and E. Shih, "Microstrip stepped impedance resonator bandpass filter with an extended optimal rejection bandwidth," *IEEE Trans. Microw. Theory Techn.*, vol. 51, no. 5, pp. 1554–1559, May 2003.
- [4] T. Yang, M. Tamura, and T. Itoh, "Compact hybrid resonator with series and shunt resonances used in miniaturized filters and balun filters," *IEEE Trans. Microw. Theory Techn.*, vol. 58, no. 2, pp. 390–402, Feb. 2010.
- [5] J.-S. Hong, *Microstrip Filters for RF/Microwave Applications*, 2nd ed. New York, NY, USA: Wiley, 2011.
- [6] R. J. Cameron, C. M. Kudsia, and R. R. Mansour, *Microwave Filters for Communication Systems-Fundamentals, Design, and Applications*, 2nd ed. New York, NY, USA: Wiley, 2018.
- [7] H. Wang and Q.-X. Chu, "An inline coaxial quasi-elliptic filter with controllable mixed electric and magnetic coupling," *IEEE Trans. Microw. Theory Techn.*, vol. 57, no. 3, pp. 667–673, Mar. 2009.
- [8] Y. Wang and M. Yu, "True inline cross-coupled coaxial cavity filters," *IEEE Trans. Microw. Theory Techn.*, vol. 57, no. 12, pp. 2958–2965, Dec. 2009.
- [9] S. Amari and G. Macchiarella, "Synthesis of inline filters with arbitrarily placed attenuation poles by using nonresonating nodes," *IEEE Trans. Microw. Theory Techn.*, vol. 53, no. 10, pp. 3075–3081, Oct. 2005.
- [10] S. Bastioli, "Nonresonating mode waveguide filters," *IEEE Microw. Mag.*, vol. 12, no. 6, pp. 77–86, Oct. 2011.
- [11] S. Amari and J. Bornemann, "Using frequency-dependent coupling to generate finite attenuation poles in direct-coupled resonator bandpass filters," *IEEE Microw. Guided Wave Lett.*, vol. 9, no. 10, pp. 404–406, Oct. 1999.

- [12] Y. He, G. Macchiarella, G. Wang, W. Wu, L. Sun, L. Wang, and R. Zhang, "A direct matrix synthesis for in-line filters with transmission zeros generated by frequency-variant couplings," *IEEE Trans. Microw. Theory Techn.*, vol. 66, no. 4, pp. 1780–1789, Apr. 2018.
- [13] J.-T. Kuo, Y.-C. Wang, and J.-W. Kuo, "Diplexer with trisections synthesized by frequency-dependent coupling," in *Proc. Asia-Pacific Microw. Conf. (APMC)*, vol. 3, Dec. 2015, pp. 1–3.
- [14] J. T. Kuo, C. L. Hsu, and E. Shih, "Compact planar quasi-elliptic function filter with inline stepped-impedance resonators," *IEEE Trans. Microw. Theory Techn.*, vol. 55, no. 8, pp. 1747–1755, Aug. 2007.
- [15] M. Ali, K.-Q. Huang, M. Swaminathan, P. M. Raj, and R. R. Tummala, "Laminated glass-based, compact inline stepped-impedance resonator bandpass filters for 5G new radio modules," *IEEE Trans. Compon., Packag., Manuf. Technol.*, vol. 11, no. 4, pp. 708–711, Apr. 2021.
- [16] K. Gong, W. Hong, Y. Zhang, P. Chen, and C. J. You, "Substrate integrated waveguide quasi-elliptic filters with controllable electric and magnetic mixed coupling," *IEEE Trans. Microw. Theory Techn.*, vol. 60, no. 10, pp. 3071–3078, Oct. 2012.
- [17] J. C. Lu, C. K. Liao, and C. Y. Chang, "Microstrip parallel-coupled filters with cascade trisection and quadruplet responses," *IEEE Trans. Microw. Theory Techn.*, vol. 56, no. 9, pp. 2101–2110, Sep. 2008.
- [18] C.-F. Chen, T.-Y. Huang, and R.-B. Wu, "Novel compact net-type resonators and their applications to microstrip bandpass filters," *IEEE Trans. Microw. Theory Techn.*, vol. 54, no. 2, pp. 755–762, Feb. 2006.
- [19] C. H. Liang and C. Y. Chang, "Compact wideband bandpass filters using stepped-impedance resonators and interdigital coupling structures," *IEEE Microw. Wireless Compon. Lett.*, vol. 19, no. 9, pp. 551–553, Sep. 2009.
- [20] B. Ren, C. Le, X. Guan, and Z. Ma, "Short-circuited stub-embedded ring resonator and its application in diplexer," *IEEE Access*, vol. 7, pp. 179266–179272, 2019.
- [21] H. N. Shaman and J.-S. Hong, "Compact wideband bandpass filter with high performance and harmonic suppression," in *Proc. Eur. Microw. Conf.*, Oct. 2007, pp. 528–531.
- [22] K. Tani and K. Wada, "Wideband bandpass filter composed of dual-path resonators using coupled-line and transmission line with inductive elements," *IEEE Microw. Wireless Compon. Lett.*, vol. 24, no. 1, pp. 14–16, Jan. 2014.
- [23] J. Zhou, Y. Rao, D. Yang, H. J. Qian, and X. Luo, "Compact wideband BPF with wide stopband using substrate integrated defected ground structure," *IEEE Microw. Wireless Compon. Lett.*, vol. 31, no. 4, pp. 353–356, Apr. 2021.
- [24] S.-W. Lan, M.-H. Weng, C.-Y. Hung, and S.-J. Chang, "Design of a compact ultra-wideband bandpass filter with an extremely broad stopband region," *IEEE Microw. Wireless Compon. Lett.*, vol. 26, no. 6, pp. 392–394, Jun. 2016.
- [25] X. Gao, W. Feng, and W. Che, "Compact ultra-wideband bandpass filter with improved upper stopband using open/shorted stubs," *IEEE Microw. Wireless Compon. Lett.*, vol. 27, no. 2, pp. 123–125, Feb. 2017.
- [26] T. W. Lin, J. T. Kuo, and S. J. Chung, "Dual-mode ring resonator bandpass filter with asymmetric inductive coupling and its miniaturization," *IEEE Trans. Microw. Theory Techn.*, vol. 60, no. 9, pp. 2808–2814, Sep. 2012.
- [27] *IE3D Simulator*, Zeland Software, Inc., Fremont, CA, USA, Jan. 1997.
- [28] D. M. Pozar, *Microwave Engineering*, 4th ed. Hoboken, NJ, USA: Wiley, 2011.
- [29] S. C. Lin, "Coupled-line filters with stub-embedded resonators using accurate admittance-transformer feeds for flexible terminations," *IEEE Trans. Microw. Theory Techn.*, vol. 62, no. 12, pp. 2911–2922, Dec. 2014.



**SHAO-CHAN TANG** was born in Taipei, Taiwan. He received the B.S. and M.S. degrees from the Department of Communications Engineering, National Chiao Tung University (NCTU), Taiwan, in 2008 and 2010, respectively. He is currently pursuing the Ph.D. degree with the Institute of Communications Engineering, National Yang Ming Chiao Tung University (NYCU), Hsinchu, Taiwan. Since 2018, he has been joined the National Chung-Shan Institute of Science & Technology (NCSIST), Taiwan. His research interests include synthesis and design of planar filters and associated RF modules for microwave and millimeter wave applications. He was a recipient of the Student Paper Prize of the 2012 Asia-Pacific Microwave Conference (APMC), Kaohsiung, Taiwan.



**PEI-CHENG CHU** was born in Kaohsiung, Taiwan, in 1995. He received the B.S. and M.S. degrees from the Department of Electronic Engineering, Chang Gung University (CGU), Taoyuan, Taiwan, in 2017 and 2019, respectively. His research interests include the analysis and design of passive microwave circuits, especially in development of innovative planar RF filters.



**JEN-TSAI KUO** (Fellow, IEEE) received the Ph.D. degree from the Institute of Electronics, National Chiao Tung University (NCTU), Hsinchu, Taiwan, in 1992. From 1984 to 2010, he was with the Department of Communication Engineering, NCTU. From 1995 to 1996, he was a Visiting Scholar with the Electrical Engineering Department, University of California at Los Angeles (UCLA). He is currently a Professor with the Department of Electronic Engineering, Chang Gung University, Taoyuan, Taiwan. His research interests include analysis and design of microwave integrated circuits and numerical techniques in electromagnetics.

He was a recipient of the Best Paper Award presented at the 2002 National Telecommunication Conference, Taiwan, the 2007 Asia-Pacific Microwave Conference (APMC) Prize, Bangkok, Thailand, and the 2008 APMC Prize, Hong Kong. He was a recipient of the 2006 Taiwan Citation Laureate presented by Thomson Scientific and the 2007 Distinguished Research Award presented by the National Science Council, Taiwan. He was an Associate Editor for the IEEE TRANSACTIONS ON MICROWAVE THEORY AND TECHNIQUES, from 2008 to 2010.



**LIN-KUN WU** (Member, IEEE) was born in Hsinchu, Taiwan, in 1958. He received the M.S. and Ph.D. degrees in electrical and computer engineering from The University of Kansas, Lawrence, Kansas, in 1982 and 1985, respectively. From November 1985 to December 1987, he was a Postdoctoral Research Associate with the Center for Research Inc., The University of Kansas, where he was involved with microwave remote sensing and computational electromagnetics. In 1988, he joined the Institute of Communications Engineering, National Chiao Tung University (NCTU), Hsinchu, where he has been a Professor, since 1993. His current research interests include computational electromagnetics, biological effects and medical applications of electromagnetic energy, and electromagnetic compatibility.



**CHUN-HUNG LIN** received the B.S. and M.S. degrees from the Department of Electronic Engineering, Ming Chuan University, Taiwan, in 2008 and 2010, respectively. He is currently pursuing the Ph.D. degree with the Department of Electronic Engineering, Chang Gung University, Taoyuan, Taiwan. His research interests include the design of passive components in microwave and millimeter communication systems.

...